IEEE Access
Multidisciplinary ⋮ Rapid Review ⋮ Open Access Journal

Received February 21, 2020, accepted March 19, 2020, date of publication March 25, 2020, date of current version April 17, 2020.

Digital Object Identifier 10.1109/ACCESS.2020.2983286

Highly Sensitive 1 × 8 Parallel Multiplexing of Ultra-Compact Integrated 1D Photonic Crystal Sensor Array Based on Silicon-on-Insulator Platform

ZHONGYUAN FU, FUJUN SUN, JIAN ZHOU, AND HUIPING TIAN

State Key Laboratory of Information Photonics and Optical Communications, Beijing University of Posts and Telecommunications, Beijing 100876, China
Beijing Key Laboratory of Space-Ground Interconnection and Convergence, Beijing University of Posts and Telecommunications, Beijing 100876, China
School of Information and Communication Engineering, Beijing University of Posts and Telecommunications, Beijing 100876, China

Corresponding author: Huiping Tian (hptian@bupt.edu.cn)

This work was supported in part by the National Natural Science Foundation of China under Grant 61634006, Grant 1372038, and Grant 61431003, in part by the National Key Technologies Research and Development Program under Grant 2017YFA0205903 and Grant 2016YFB0402405, and in part by the Fund of Joint Laboratory for Undersea Optical Networks and BUPT Excellent Ph.D. Students Foundation, China, under Grant CX2016207.

ABSTRACT We design a 1 × 8 highly sensitive ultra-compact on-chip integrated sensor array consisting of a 1 × 8 power splitter, eight one-dimensional photonic crystal slot nanobeam cavities (1DPC-SNCs) connected by additional 1D photonic crystal tapered nanobeam bandgap filters (1DPC-TNBF), and an 8 × 1 power combiner. The performance of the device is numerically demonstrated by three-dimensional finite-difference-time-domain (3D-FDTD) method. The whole structure is lying on top of a 2 μm buried silicon oxide layer, while remaining high sensitivities (over 400 nm/RIU) of the eight sensors, simultaneously. The proposed 1DPC-SNCs can reach a high-quality factor of 3.6×10^5. On account of the additional band-stop filters and the 8 × 1 power combiner, eight sensing segments interrogated simultaneously by one input and one output port is realized, with the ultra-compact footprint of 64×16 μm^2 (26×16 μm^2 in sensing region). Therefore, this design is a promising platform for realizing large-scale photonic integrated circuits with high integration density, especially for ultra-compact multiple on-chip sensing.

INDEX TERMS Photonic crystals, optical sensors, sensor arrays, integrated optics.

I. INTRODUCTION

Optical devices have been widely researched in recent years. The most exploited fields are based on surface plasmonics [1], Mach–Zehnder interferometers [2], ring resonators [3], whispering gallery mode [4] and photonic crystal (PhC) cavities [5]. Among them, PhC sensors based on silicon-on-insulator (SOI) obtain plenty of attention with the advantages of strong light-matter interaction, high Q-factor, and ease of on-chip integration. As an important field of nano- and micrometer-scale optoelectronic devices, silicon has intrinsic advantages in photonic material systems, for the reason of high refractive index (RI) contrast with silicon dioxide, which provides silicon photonic devices, especially silicon PhC structures the ability to realize ultra-compact and high-sensitive bio-chemical sensors [6]–[11].

In order to enhance sensitivity and reduce mode volume, slot photonic crystal cavities have been extensively used in the design of ultra-compact optical sensors. Hoang *et al.* designed an SOI slotted photonic crystal cavities with Q/V factors above 800000 [12]. Zhang *et al.* presented the design of a femtogram scale double-slot photonic crystal optomechanical cavity, reducing the mechanical effective masses close to 4 fg [13]. However, those designs are based on 2D PhC, leading to a large footprint (for example, the footprint of the slot 2D PhC device in [12] is larger than 20×4.5 μm^2), which is not suitable for high-density integration. Li *et al.* investigated a high-Q and high-sensitivity one-dimensional photonic crystal slot nanobeam cavity sensors with the sensitivity as high as 851 nm/RIU and Q-factor of 96465 [14].

The associate editor coordinating the review of this manuscript and approving it for publication was Md Selim Habib.

Zhou *et al*. designed parabolically tapered coupled two photonic crystal nanobeam slot cavities with a sensitivity of 415 nm/RIU and Q-factor of 1.14×10^7 [15]. Wang *et al.* designed slot-mode photonic crystal cavities with a sensitivity of 451 nm/RIU and Q-factor >7000 [16]. Although high performance is obtained in those sensors, the suspended condition results in fragility and difficulty in the development of large integration platform designed for SOI wire waveguides [17].

A new trend of PhC sensor design is realizing multiple sensing sites, which increases the efficiency of samples probed at one time. In order to achieve multiple sensing, several kinds of sensor arrays based on 1D PhC cavities and 2D PhC cavities [18]–[28] have been investigated. Mandal *et al*. introduced nanoscale optofluidic sensor arrays (NOSAs) using side-coupled 1D PhC cavities, with the detection limit of 7×10^{-5} [18]. Yang *et al*. presented side-coupled nanoscale photonic crystal sensor arrays (NPhCSAs) on a 2D PhC slab [19]. However, those structures are limited in Q-factor of 10^4 and sensitivity of 14.96 nm/fg and 115.60 nm/RIU, respectively. Connected in parallel without spectrum overlap, the cavities used in sensor arrays must have large free spectral ranges (FSR). Therefore, Zhou *et al*. presented an efficient method for the sensor array of high-sensitivity single-slot photonic crystal nanobeam cavities (PCNCs) by adding a W1 PhC slab as a band-stop filter [20], with limited Q-factor. Yang *et al*. proposed an ultra-compact integrated sensor array by using 1D photonic crystal nanobeam band-stop filters [21], however, the sensitivity is smaller than 150 nm/RIU. Furthermore, the $1 \times n$ taper-type equal power splitter displayed in the Ref [21] should satisfy the single mode of the input light. However, single mode is generally concentrated in the finite range in the middle of such a waveguide, which results in a quite wide input waveguide when splitter number n is larger than 4. In addition, for the given wavelength, it is difficult to realize single mode in such a wide waveguide in practical.

In order to overcome the drawback and limitation of the sensors mentioned above, a kind of a modified high Q and high sensitivity 1D photonic crystal slot nanobeam cavity, and a low sidelobe 1D photonic crystal tapered nanobeam bandgap filter (1DPC-TNBF) based on SOI are designed and demonstrated in this paper. By connecting the proposed cavity and filter in series, a sensing segment is proposed and only selected targeted mode (∼1540nm) is observed in a broad wavelength range. Furthermore, parallel multiplexing of a 1×8 highly sensitive ultra-compact integrated 1D photonic crystal sensor array based on SOI is designed by connecting the eight sensing segments with a high transmittance single mode cascaded Y-junction 1×8 power splitter and a high transmittance 8×1 power combiner. The whole structure is lying on top of a 2 μm buried silicon oxide layer, without suspended area, for ease of fabrication. By using the 3D-FDTD method, the output transmission with only eight resonant peaks is obtained. The measured bulk RI sensitivities of the eight sensing segments are all over 400 nm/RIU, which are relatively high in multiple sensing. In addition, owing to the miniaturized geometries, the footprint of the whole structure is only 64×16 μm^2 (26×16 μm^2 in sensing region), which is much more compact compared to 2D PhC side-coupled sensor arrays [19], [22] and other 1D PhC sensor arrays [18], [21].

II. 1DPC-SNC DESIGN AND ANALYSIS

The traditional 1DPC-SNCs are usually set in a suspended area in order to enhance the sensitivity and Q-factor. However, this kind of design is difficult in physical implementation and fragile in the environment. Here, a modified 1DPC-SNC is designed on an asymmetric air/Si/SiO_2 slab with no suspended area. This design is more suitable for the development of large-scale integrated circuits based on SOI platform [12].

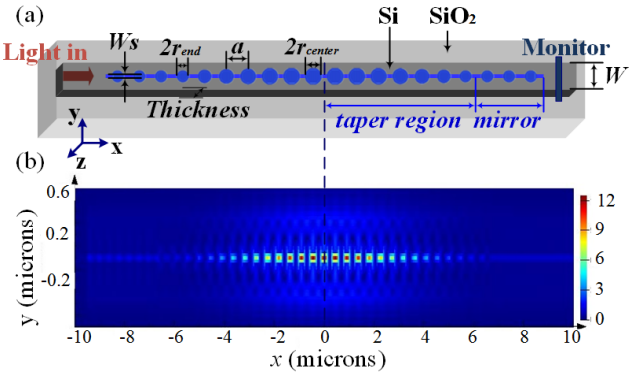

FIGURE 1. (a) Schematic of the proposed 1DPC-SNC. The cavity is symmetric with respect to its center (blue dashed line). r_{center} and r_{end} are the radii of the air holes that are tapered parabolically from the center to both ends. (b) Electric field intensity of the resonant mode calculated by the 3D-FDTD method.

The schematic of the 1DPC-SNC is shown in Fig. 1(a). The PhC cavity, with silicon slab thickness (T) of 220 nm, is lying on top of a 2 μm buried silicon oxide layer with no air-bridge design. The width (W) of the nanobeam is 650 nm and the slot width (Ws) is set as 40 nm, which is the narrowest width of a slot that could be etched vertically and thoroughly in the [16]. The optical field strongly localized inside the low index region is achieved when the slot is exploited which enhances overlaps sufficiently with the analytes. The periodicity (a) of the PhC cavity, defined as the hole-to-hole distances, is 450 nm with circular air holes in different radii (R). 1DPC-SNCs suspended in the air usually have a large filling fraction (defined as the ratio of the area of the air-hole to the area of the unit cell). The band diagrams are simulated by the 3D-FDTD method with the commercial software Lumerical [30]. To automatically match the periodicity of the physical structure, Lumerical FDTD solutions use non-uniform mesh. The mesh accuracy is set to be 4 (corresponding to 1/18 of the shortest wavelength in the material). Perfectly matched layer (PML) boundaries are set in y and z directions, and in *the* x-direction is Bloch boundaries. The 1DPC-SNC is optimized by using the

deterministic high-Q design method [31]. To create the Bragg mirror with a linear change in the mirror strength γ, the air-holes radii are parabolically tapered from $r_{center} = 152.6$ nm to $r_{end} = 125.8$ nm, i.e., $r(t) = r_{center} + i^2(r_{end} - r_{center})/i_{max}^2$, ($i$ increases from 0 to i_{max}), in which the filling fraction (f) is from 0.25 to 0.17. The mirror strength γ can be calculated using $\sqrt{(w_2 - w_1)^2/(w_2 + w_1)^2 - (w_{res} - w_0)^2/w_0^2)}$ for different filling fractions, where w_{res} is the proposed target resonance, and w_1, w_2, and w_0 are the dielectric band edge, air band edge, and midgap frequency of each segment, respectively [30]. In order to set the target wavelength to 1550 nm, the periodicity of the cavity is 450 nm. The mirror strengths of different air hole radii are shown in Fig. 2(b) and the highest value is obtained when the filling fraction is 0.19. However, the frequency interval between the zeroth and first mode of the proposed cavity is smaller than the case when the filling fraction in the edge is 0.17, which leads to the latter more suitable for multiple sensing.

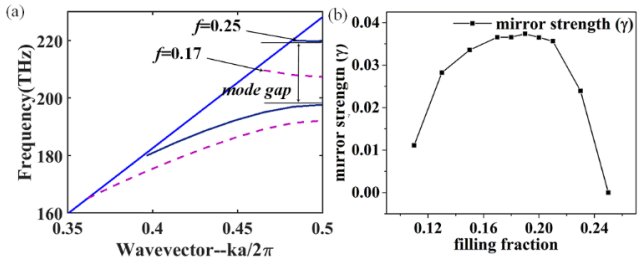

FIGURE 2. (a) TE band diagram of the 1DPC-SNC with $f = 0.25$ (blue solid line) and $f = 0.17$ (purple dashed line). The mode gap when $f = 0.25$ is displayed. (b) Mirror strengths at different filling fractions.

In order to achieve a radiation-Q limited cavity [31], the number of Gaussian mirrors is $i_{max} = 30$ with 15 additional mirror segments at both edges of the Gaussian mirror. By using the 3D-FDTD method, a high Q-factor of 3.6×10^5 is obtained. The resonant wavelength of the cavity mode is very close to but slightly higher than, the dielectric band edge of the central mirror segment. This can be attributed to the linearly decreasing the filling fraction of the mirror, which results in an increased overlap between the cavity mode and dielectric material [32]. The electric field distribution profile is shown in Fig. 1(b). The light is strongly confined in the slot region, which enhances the sensitivity of the sensor significantly.

To verify the sensing performances of the proposed 1DPC-SNC, the sensitivity is calculated by 3D-FDTD simulations. The mesh accuracy is set to be 3 (corresponding to 1/14 of the shortest wavelength in the material), and PML boundaries are set in x, y and z directions. These settings are used in all the following simulations. To reduce the simulation time and further comprehend the properties of the proposed sensor, we used a high-transmission but low-Q geometry. The number of Gaussian mirrors is $i_{max} = 15$ with 5 additional mirror segments at both edges of the Gaussian mirror, possessing a moderate Q-factor.

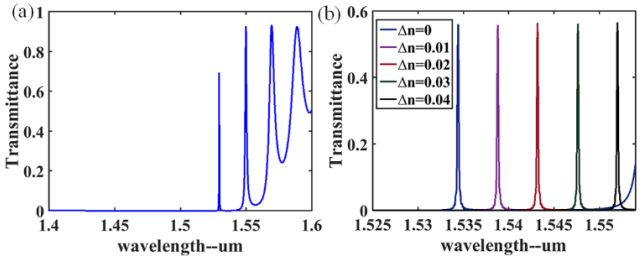

FIGURE 3. (a) The entire transmission spectrum of the proposed 1DPC-SNC sensor calculated by 3D-FDTD simulation. The structure consists of the number of Gaussian mirror $i_{max} = 15$ with 5 additional mirror segments at both edges. (b) Transmission spectra of the 1DPC-SNC when the background index changes from RI = 1.00 RIU to RI = 1.04 RIU.

The bulk RI sensitivity of the sensor is defined as $S = \Delta\lambda/\Delta n$, where $\Delta\lambda$ is the shift of resonant wavelength and Δn is the change in RI. The transmission spectrum of the optimized 1DPC-SNC sensor is shown in Fig. 3(a), and the sensitivity of 439 nm/RIU can be calculated according to the transmission spectra shown in Fig. 3(b), where the change of RI is from 1.00 to 1.04 RIU in the air environment. The calculated sensitivity is much higher than the sensor in the Ref [21] and other sensors designed by air/Si/SiO_2 slabs [18], [19], [27].

In the practical fabrication of the proposed 1DPC-SNC, acceptable fabrication tolerance should be further discussed in detail. Therefore, we consider the effect of the fabrication roughness (e.g. slot width) in our design. The simulation is done in the air environment, assuming a random distribution of slot width from −1 to 1, −2 to 2, −3 to 3, and −4 to 4 nm, respectively. As shown in Fig. 4(b), the shift of resonant wavelength and the decrease of Q-factor are not obvious, which should be achievable when the fabrication perturbation is taken into consideration.

Therefore, the advantages of high Q-factor, high sensitivity, small mode volume and ease of fabrication make the proposed 1DPC-SNC a promising candidate for on-chip gas sensing arrays.

III. TAPERED BAND-STOP FILTER DESIGN AND ANALYSIS

As shown in Fig. 3(a), the proposed 1DPC-SNC has several resonant wavelengths in the transmission spectrum, which makes the cavity difficult in realizing multiple sensing. In order to overcome this limitation, several solutions have been proposed in recent researches. 2D PhCW bandpass filter [20] with comparatively narrow stopband and 1-D PC nanobeam bandstop filter [21] disadvantageous in drastic sidelobe fluctuation cannot satisfy the requirement of high sensitivity large-scale sensor arrays. Huang *et al.* design an ultra-compact, broadband tunable optical bandstop filters based on a multimode one-dimensional photonic crystal waveguide, while the filter will complicate the sensor

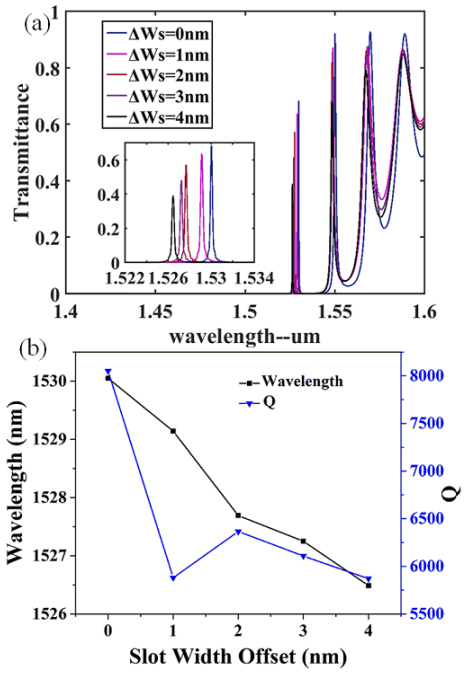

FIGURE 4. (a) Transmission spectra of the 1DPC-SNC with different slot width variation from $\Delta Ws = 0$ nm to $\Delta Ws = 4$ nm. (b) 3D-FDTD simulation of Q-factors and wavelength shift considering the effect of fabrication roughness.

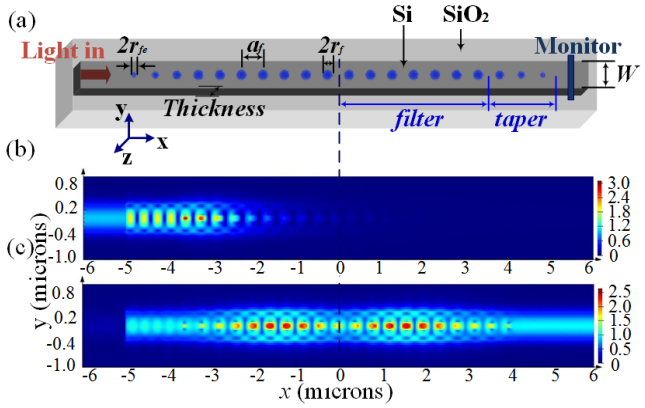

FIGURE 5. (a) Schematic of the proposed 1DPC-TNBF. The filter is symmetric with respect to its center (blue dashed line). r_f and r_{fe} are the radii of the air holes in the filter region and the end of taper region. (b) Electric field intensity of the light in stopband at the wavelength of 1609.81 nm. (c) Electric field intensity of the light in the passband at the wavelength of 1501.55 nm.

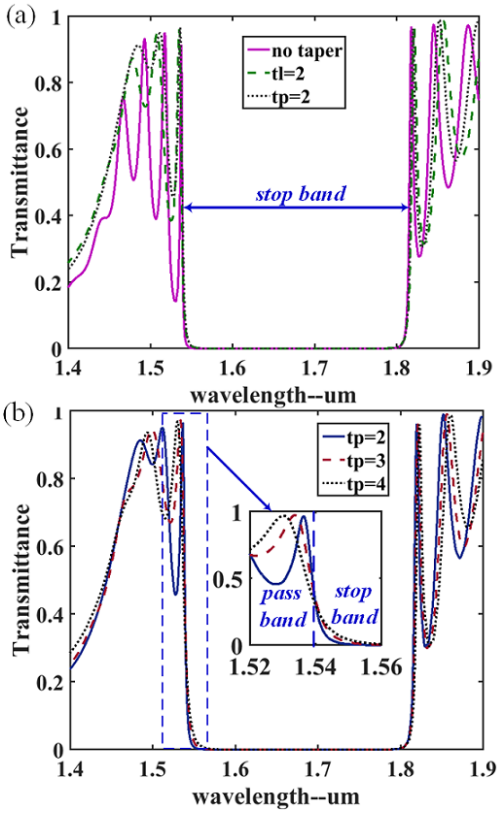

FIGURE 6. (a) The transmission spectra of three different taper profiles calculated by 3D-FDTD simulation: no taper, radius linear taper (t_l) and proportion linear taper (t_p) with a purple solid line, green dashed line and gray dotted line, respectively. (b) The transmission spectra of different taper region lengths in two ($t_p = 2$), three ($t_p = 3$) and four ($t_p = 4$) mirrors with blue solid line, red dashed line and black dotted line, respectively.

array design [34]. Other filters, such as microring resonators (MRRs) [35], arrayed waveguide gratings (AWGs) [36], and waveguide Bragg gratings (WBGs) [37], usually have too large footprints compared with the proposed 1DPC-SNC.

In order to solve the problems above, a modified 1D photonic crystal tapered nanobeam bandgap filter (1DPC-TNBF) with low sidelobe and simple design for integration of 1DPC-SNC is proposed based on SOI. The schematic of the proposed 1DPC-TNBF is shown in Fig. 5(a). To fit the scale of the 1DPC-SNC, the silicon slab thickness (T) and the width (W) of the waveguide are set to 220 nm and 650 nm, respectively, the same as the cavity designed in Sec. 2. The filter contains 20 mirrors, with varied filter region and taper region. The periodicity (a_f) is 400 nm, and the radii of the air holes in the filter region (r_f) are set to 90 nm. A large stopband is obtained between the wavelength from 1550 nm to 1800 nm. By adjusting the periodicity of 1DPC-TNBF, an arbitrary stopband can be obtained. The influence of different taper profiles and different taper lengths are analyzed. It is pointed out previously that the serious sidelobes of TE mode are mainly caused by the mismatch between Bloch mode and waveguide mode at the interface between a strip waveguide and 1D PhCW [34]. Therefore, a taper region between the two waveguides can suppress the sidelobes significantly.

As shown in Fig. 5(a), only two mirrors of the taper region (t_{max}) at each side enable a remarkable improvement in suppressing sidelobes. The transmission spectra of two different taper profiles, radius linear taper, and proportion linear taper are also displayed in Fig. 6(a) with green dashed line and gray dotted line, respectively. The air hole radius of linear taper is defined as $r(t) = r_f \cdot (t_{max} + 1 - t)/(t_{max} + 1)$ (t increases from 0 to t_{max}). In particular, the air hole radius at

the end of the taper region is calculated as $r_{fe} = r_f/(t_{max}+1)$. The air hole radius of proportion linear taper is defined as $r(t) = r_f \cdot \sqrt{(t_{max}+1-t)/(t_{max}+1)}$. The radius of the outermost air hole is calculated as $r_{fe} = r_f/\sqrt{(t_{max}+1)}$. It can be observed that the filter with proportion linear taper gets flatter sidelobes with the same taper region length, because of the reduction in mode mismatch.

The transmission spectra of different taper region lengths in two, three and four mirrors are shown in Fig. 6(b) with a blue solid line, red dashed line and black dotted line, respectively. The suppression of sidelobes is better when the taper region gets longer, sacrificing in less sharpness between passband and stopband. For the trade-off, the length of three mirrors in each taper region is selected for an effective bandstop filter to suppress the higher order modes of the 1DPC-SNC, while avoids the severe degeneracy of fundamental mode. The proposed 1DPC-TNBF is quite suitable for realizing highly sensitive 1 × 8 parallel multiplexing of an ultra-compact integrated sensor array.

IV. THE INTEGRATED 1 × 8 PARALLEL MULTIPLEXING SENSOR ARRAY DESIGN AND PROPERTIES ANALYSIS

Based on the design and property analysis in Sec. 2 and Sec. 3, a kind of sensor structure suitable for multiple sensing is designed by connecting the proposed 1DPC-SNC and 1DPC-TNBF in cascade. The schematic of the integration is shown in Fig. 7(a). The silicon slab thickness (T) and the width (W) of the waveguide are set to 220 nm and 650 nm, respectively, the same as the cavity and filter designed above. The 1DPC-SNC contains 10 Gaussian mirrors with 5 additional mirror segments at both edges with the periodicity (a) of 450 nm. The air hole radii are parabolically tapered from $r_{center} = 152.6$ nm in the center to $r_{end} = 125.8$ nm on both sides with a slot ($Ws = 40$ nm) in the middle, which is symmetric to the cavity center. The filter contains 20 mirrors, with three mirrors of proportion linear taper region on each side. The periodicity $a_f = 403$ nm, the radii of the air holes in filter region $r_f = 90$ nm, and the air hole radii are proportion linear tapered from $r_f = 90$ nm in the center to $r_{fe} = 45$ nm on each side. The electric field intensity of the resonant mode at the wavelength of 1544 nm is shown in Fig. 7(b).

The transmission spectra of the cavity with and without a filter are shown in Fig. 8(a). As expected, in the case of a cascaded device, the higher order resonant modes in the stopband are filtered out and have no effect on the selected fundamental resonant mode. Considering the practical fabrication of the proposed cascaded device, the transmission spectra of 1DPC-SNC cascaded with 1DPC-TNBF in different periodicities (a_f) are shown in Fig. 8(b). When a_f is smaller than 401 nm, the fundamental resonant mode is suppressed, while the higher order modes are not filtered out completely when a_f is larger than 405 nm.

According to the simulation results above, the design of realizing 1 × 8 parallel multiplexing of highly sensitive integrated sensor array based on SOI is proposed and demonstrated. The schematic of the proposed sensor array is shown in Fig. 9. Each channel consists of cascaded one 1DPC-SNC and one 1DPC-TNBF with a slight difference in periodicity, and the adjacent channels are separated by air-gap separations. The eight channels are connected in parallel by using a 1 × 8 beam splitter and an 8 × 1 multiple mode power combiner in the input and output port, respectively. The width of the input and S-bend waveguides is set to 420 nm to remain single mode, which is narrower than the cavity width. Therefore, a taper with a length of 1 μm is added between the S-bend waveguides and the cavities to reduce mode mismatch. The width of the output waveguide is 3.36 μm, and multiple waveguide modes will be excited. In a practical

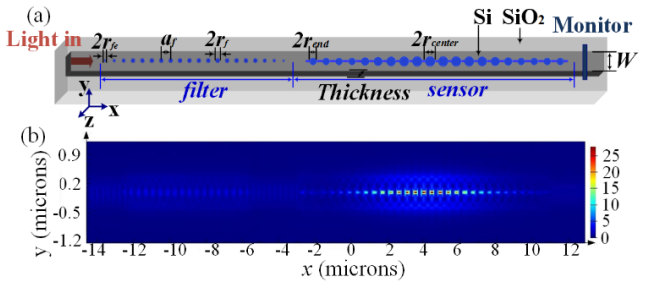

FIGURE 7. (a) Schematics of the integrated device connecting the proposed 1DPC-SNC and 1DPC-TNBF in cascade. (b) Electric field intensity of the resonant mode calculated by the 3D-FDTD method.

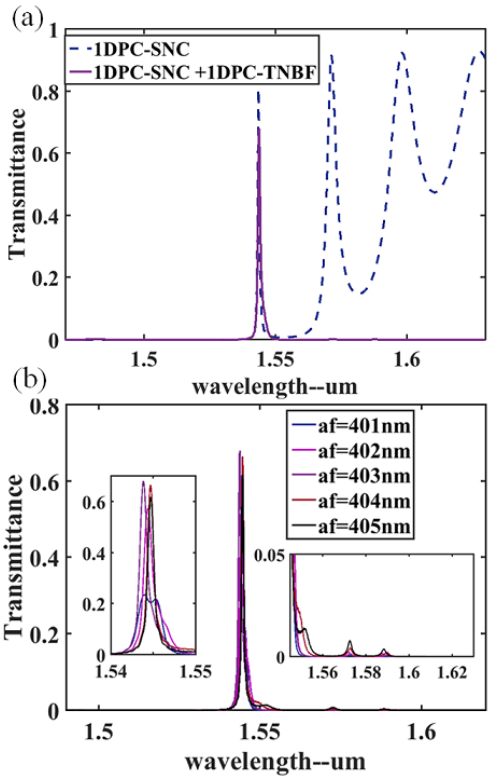

FIGURE 8. (a) The transmission spectra of the 1DPC-SNC with and without 1DPC-TNBF ($a_f = 403$ nm) setting in cascade calculated by 3D-FDTD simulation. (b) the transmission spectra of 1DPC-SNC cascaded with 1DPC-TNBF in different periodicities (a_f) from 401 nm to 405 nm.

TABLE 1. The parameters of the eight sensing segments.

Eight sensing segments	1	2	3	4	5	6	7	8
Cavity periodicity (nm)	426	434	442	450	458	466	474	482
Filter periodicity (nm)	388	393	397	403	412	417	423	--
Sensitivity (nm/RIU)	405	422	419	445	461	443	454	452

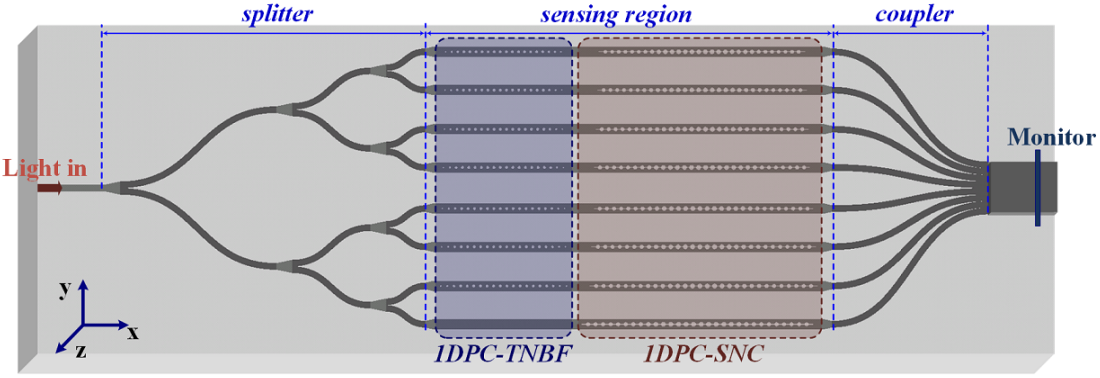

FIGURE 9. The Schematic of highly sensitive 1 × 8 parallel multiplexing of ultra-compact integrated sensor array by utilizing a 1 × 8 power splitter, eight 1D photonic crystal slot nanobeam cavities (1DPC-SNCs) connected by additional band-stop filters and an 8 × 1 coupler.

implementation, in order to achieve highly efficient coupling between the input/output fiber lens and the sensor array, a second E-beam lithography can be performed with SU8-2002 E-beam resist fabricating the input/output bus waveguides [38]. The splitter is much more compact and avoids multiple interferences at the input port compared with the $1\times n$ taper-type equal power splitter mentioned in the [21].

The eight cavities are in different periodicities but remain the silicon slab thickness (T), the width of the waveguide (W), slot width (Ws) and the filling fraction (f) invariable. The seven 1DPC-TNBFs are also different in periodicity while remaining the air hole radii (r_f and r_{fe}) unchanged. Considering the detection range limit, the filter for the selected resonant mode at the longest wavelength is unnecessary. Therefore, only seven filters are used in the proposed 1 × 8 sensor array. The filters are added in the sensing region, so the band edges of the filters will shift along with the cavity resonances, resulting in more range for detecting RI change. By applying these processes, eight selected resonant modes in different wavelengths are obtained. The method by changing periodicities of 1D-PhC nanobeams (lattice constant in 2D-PhC) is a simple and effective way to realize stabilized, performance controlled resonant wavelengths for multiple sensing. The cavity periodicities, filter periodicities of eight sensing segments are shown in Table 1.

The transmission spectra of eight integrated devices consisting of cascaded one 1DPC-SNC and one 1DPC-TNBF calculated individually are shown in Fig. 10(a). Eight selected modes with almost the same interval and high transmittance are obtained. Because of the different sensitivities in the 1DPC-SNC and 1DPC-TNBF, the periodicities chosen for

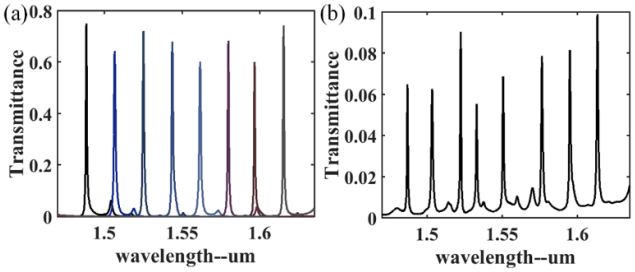

FIGURE 10. (a) The transmission spectra of individually calculated eight integrated devices consisting of cascaded one 1DPC-SNC and one 1DPC-TNBF. (b) The transmission spectrum of the highly sensitive 1 × 8 parallel multiplexing of ultra-compact integrated sensor array calculated by 3D-FDTD simulation.

1DPC-TNBFs are a little larger than the periodicities obtain the best performances. Otherwise, the fundamental resonant mode will be suppressed when the RI increases. Therefore, some small peaks can be observed. The transmission spectrum for each channel of the proposed 1 × 8 sensor array is shown in Fig. 10(b). As expected, when eight sensing segments are set in parallel, the transmission spectrum of the sensor array exhibits eight separated resonant peaks. The little wavelength difference of sensing segment-4 and segment-5 can be observed from Fig. 10(a) and Fig. 10(b), which is mainly caused by the deficiency of simulation accuracy in such a large simulation region.

To investigate the multiple sensing performances of the proposed 1 × 8 sensor array, the device is characterized by changing bulk RI of the sensing environment. The transmission spectra of the proposed sensor array are shown in

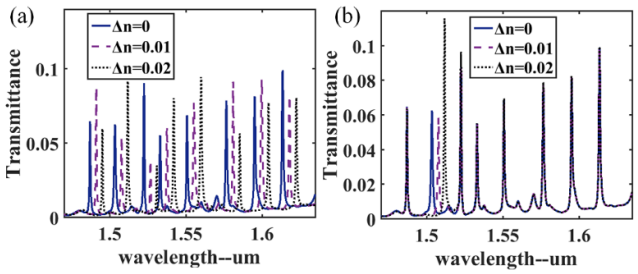

FIGURE 11. The transmission spectra of the proposed 1 × 8 parallel multiplexing sensor array when (a) changing the RI of all eight sensing segments. (b) only segment-2 is subjected to the changes in RI.

Fig. 10(a) when the bulk RI of all eight sensing segments are changed. The eight sensing segments are interrogated with only one input and one output waveguide. The change of RI is from 1.00 to 1.02 RIU in air environment, and the RI change has a linear variation with the wavelength shift of eight resonant peaks. Fig. 11(a) shows that when RI is increased, the resonant peak of each sensor shifts towards longer wavelengths (red-shift). The limitation of the index variation of the integrated sensor array is calculated at around 0.02 RIU, on the bases of the intervals between eight resonant peaks. The limitation satisfies the need for gas sensing [39]. The reason for the variants of the peak heights in different surroundings is mainly because of the different sensitivities between the 1DPC-SNCs and the 1DPC-TNBFs.

The calculated bulk RI sensitivities of the eight sensing segments are shown in Table 1. The sensitivities are all over 400 nm/RIU, which are nearly improved by a factor of four compared with the sensitivities of the sensor array in the Ref [21].

In order to further confirm the independence of all sensing segments, the bulk RI around the sensing segment-2 is changed while other sensing segments remain invariant. The transmission spectra of the device when only segment-2 is subjected to the changes in RI from 1.00 to 1.02 RIU are shown in Fig. 11(b). The transmission spectra verify that the resonant peaks are independent, which means the RI change in one of the sensing segments does not perturb the others. This allows the implementation of a simple but functional integrated sensor array for parallel multiplexing.

In a practical implementation, the interface of different 1DPC-SNCs with different gas channels is one of the challenges for ultra-compact sensing applications. The challenge can be solved by using parallel microfluidic channels (suitable for a 26 μm long footprint calculated in each sensing segment) which can be fabricated by a soft lithography technique with polydimethylsiloxane (PDMS) using replica molding of a SU-8 template [40]. Meantime, the improvement of electron beam lithography enables multiplexed 1DPC-SNC sensor arrays in a mechanically-robust approach on a monolithic silicon chip. Therefore, the proposed sensor array is a potential candidate for gas concentration detection.

V. CONCLUSION

In summary, a 1 × 8 highly sensitive ultra-compact integrated sensor array for parallel multiplexing is designed and demonstrated. By using the 3D-FDTD method, the calculated Q-factor of the proposed 1DPC-SNC is 3.6×10^5, and the bulk RI sensitivities of the eight 1DPC-SNCs are all over 400 nm/RIU. The whole structure is on an asymmetric air/Si/SiO_2 slab with no suspended area, which enhances the robustness and reduces the fabrication difficulty simultaneously. Large-scale parallel multiplexing interrogated simultaneously by one input and one output port is realized, which means multiple different targets can be detected independently at the same time. In particular, the ultra-compact footprint of 64 × 16 μm^2 (26 × 16 μm^2 in the sensing region) is obtained in the whole integrated device. Attributing to high sensitivity, small footprint, high integration density, and ease of fabrication, the proposed 1 × 8 sensor array is potentially an ideal platform for large-scale multiple on-chip sensing.

REFERENCES

[1] K. Bian, H. Schunk, D. Ye, A. Hwang, T. S. Luk, R. Li, Z. Wang, and H. Fan, "Formation of self-assembled gold nanoparticle supercrystals with facet-dependent surface plasmonic coupling," *Nature Commun.*, vol. 9, no. 1, p. 2365, Dec. 2018.

[2] H. C. A. S. G. Vasconcelos, J. M. M. M. D. Almeida, C. M. T. Saraiva, P. A. D. S. Jorge, and L. C. C. Coelho, "Mach–Zehnder interferometers based on long period fiber grating coated with titanium dioxide for refractive index sensing," *J. Lightw. Technol.*, vol. 37, no. 18, pp. 4584–4589, Sep. 15, 2019.

[3] F. Copie, M. T. M. Woodley, L. Del Bino, J. M. Silver, S. Zhang, and P. Del'Haye, "Interplay of polarization and time-reversal symmetry breaking in synchronously pumped ring resonators," *Phys. Rev. Lett.*, vol. 122, no. 1, 2019, Art. no. 013905.

[4] S. Frustaci and F. Vollmer, "Whispering-gallery mode (WGM) sensors: Review of established and WGM-based techniques to study protein conformational dynamics," *Current Opinion Chem. Biol.*, vol. 51, pp. 66–73, 2019.

[5] M. Clementi, K. Debnath, M. Sotto, A. Barone, A. Z. Khokhar, T. D. Bucio, S. Saito, F. Y. Gardes, D. Bajoni, and M. Galli, "Cavity-enhanced harmonic generation in silicon rich nitride photonic crystal microresonators," *Appl. Phys. Lett.*, vol. 114, no. 13, Apr. 2019, Art. no. 131103.

[6] P. Xu, J. Zheng, J. Zhou, Y. Chen, C. Zou, and A. Majumdar, "Multi-slot photonic crystal cavities for high-sensitivity refractive index sensing," *Opt. Express*, vol. 27, no. 3, pp. 3609–3616, Feb. 2019.

[7] A. M. Ahmed and A. Mehaney, "Ultra-high sensitive 1D porous silicon photonic crystal sensor based on the coupling of Tamm/Fano resonances in the mid-infrared region," *Sci. Rep.*, vol. 9, no. 1, Dec. 2019, Art. no. 6973.

[8] D. Yang, P. Zhang, H. Tian, Y. Ji, and Q. Quan, "Ultrahigh-Q and low-mode-volume parabolic radius-modulated single photonic crystal slot nanobeam cavity for high-sensitivity refractive index sensing," *IEEE Photon. J.*, vol. 7, no. 5, pp. 1–8, Oct. 2015.

[9] T. Nakamura, Y. Takahashi, Y. Tanaka, T. Asano, and S. Noda, "Improvement in the quality factors for photonic crystal nanocavities via visualization of the leaky components," *Opt. Express*, vol. 24, no. 9, pp. 9541–9549, May 2016.

[10] Y.-H. Chen, W.-H. Shi, L. Feng, X.-Y. Xu, and M.-Y. Shang-Guan, "Study on simultaneous sensing of gas concentration and temperature in one-dimensional photonic crystal," *Superlattices Microstruct.*, vol. 131, pp. 53–58, Jul. 2019.

[11] D. Yamashita, Y. Takahashi, T. Asano, and S. Noda, "Raman shift and strain effect in high-Q photonic crystal silicon nanocavity," *Opt. Express*, vol. 23, no. 4, pp. 3951–3959, Feb. 2015.

[12] T. H. C. Hoang, W. Zhang, S. F. Serna-Otálvaro, C. Caër, X. Le Roux, L. Vivien, and E. Cassan, "SOI slotted photonic crystal cavities spanning from 1.3 to 1.6 μm with Q/V factors above 800 000," *IEEE Photon. Technol. Lett.*, vol. 27, no. 20, pp. 2138–2141, Oct. 15, 2015.

[13] H. Zhang, Y. Zhang, G. Gao, X. Zhao, Y. Wang, Q. Huang, J. Yu, and J. Xia, "Design of a femtogram scale double-slot photonic crystal optomechanical cavity," *Opt. Express*, vol. 23, no. 18, pp. 23167–23176, Sep. 2015.
[14] T. Li, D. Gao, D. Zhang, and E. Cassan, "High-*Q* and high-sensitivity one-dimensional photonic crystal slot nanobeam cavity sensors," *IEEE Photon. Technol. Lett.*, vol. 28, no. 6, pp. 689–692, Mar. 15, 2016.
[15] J. Zhou, H. Tian, L. Huang, Z. Fu, F. Sun, and Y. Ji, "Parabolic tapered coupled two photonic crystal nanobeam slot cavities for high-FOM biosensing," *IEEE Photon. Technol. Lett.*, vol. 29, no. 16, pp. 1281–1284, Aug. 15, 2016.
[16] C. Wang, Q. Quan, S. Kita, Y. Li, and M. Lončar, "Single-nanoparticle detection with slot-mode photonic crystal cavities," *Appl. Phys. Lett.*, vol. 106, no. 26, Jun. 2015, Art. no. 261105.
[17] J. Vuckovic, M. Loncar, H. Mabuchi, and A. Scherer, "Optimization of the Q-factor in photonic crystal microcavities," *IEEE J. Quantum Electron.*, vol. 38, no. 7, pp. 850–856, Jul. 2002.
[18] S. Mandal and D. Erickson, "Nanoscale optofluidic sensor arrays," *Opt. Express*, vol. 16, no. 3, pp. 1623–1631, 2008.
[19] D. Yang, H. Tian, and Y. Ji, "Nanoscale photonic crystal sensor arrays on monolithic substrates using side-coupled resonant cavity arrays," *Opt. Express*, vol. 19, no. 21, pp. 20023–20034, Oct. 2011.
[20] J. Zhou, L. Huang, Z. Fu, F. Sun, and H. Tian, "Multiplexed simultaneous high sensitivity sensors with high-order mode based on the integration of photonic crystal 1×3 beam splitter and three different single-slot PCNCs," *Sensors*, vol. 16, no. 7, p. 1050, 2016.
[21] D. Yang, C. Wang, and Y. Ji, "Silicon on-chip 1D photonic crystal nanobeam bandstop filters for the parallel multiplexing of ultra-compact integrated sensor array," *Opt. Express*, vol. 24, no. 15, pp. 16267–16279, Jul. 2016.
[22] Y. Zou, S. Chakravarty, L. Zhu, and R. T. Chen, "The role of group index engineering in series-connected photonic crystal microcavities for high density sensor microarrays," *Appl. Phys. Lett.*, vol. 104, no. 14, 2015, Art. no. 141103.
[23] Y. Zou, S. Chakravarty, W.-C. Lai, C.-Y. Lin, and R. T. Chen, "Methods to array photonic crystal microcavities for high throughput high sensitivity biosensing on a silicon-chip based platform," *Lab Chip*, vol. 12, no. 13, pp. 2309–2312, 2012.
[24] D. Yang, H. Tian, and Y. Ji, "Nanoscale low crosstalk photonic crystal integrated sensor array," *IEEE Photon. J.*, vol. 6, no. 1, pp. 1–7, Feb. 2014.
[25] H. Yan, Y. Zou, S. Chakravarty, C. Yang, Z. Wang, N. Tang, D. Fan, and R. T. Chen, "Silicon on-chip bandpass filters for the multiplexing of high sensitivity photonic crystal microcavity biosensors," *Appl. Phys. Lett.*, vol. 106, no. 12, 2015, Art. no. 121103.
[26] P. Zhang, H. Tian, D. Yang, Q. Liu, J. Zhou, L. Huang, and Y. Ji, "Radius vertical graded nanoscale interlaced-coupled photonic crystal sensors array," *Opt. Commun.*, vol. 355, pp. 331–336, Nov. 2015.
[27] Z. Fu, J. Zhou, L. Huang, F. Sun, and H. Tian, "Performance investigation of side-coupled interlaced symmetric-shaft-shape photonic crystal sensor arrays," *Opt. Commun.*, vol. 381, pp. 146–151, Dec. 2016.
[28] S. Makino, T. Fujisawa, and K. Saitoh, "Enhancement of optical nonlinearity in coupled resonator optical waveguide based on slotted 1-D photonic crystal cavity," *IEEE Photon. J.*, vol. 7, no. 6, pp. 1–8, Dec. 2015.
[29] E. Kuramochi, H. Taniyama, T. Tanabe, K. Kawasaki, Y. G. Roh, and M. Notomi, "Ultrahigh-Q one-dimensional photonic crystal nanocavities with modulated mode-gap barriers on SiO_2 claddings and on air claddings," *Opt. Express*, vol. 18, no. 15, pp. 15859–15869, 2010.
[30] Q. Quan and M. Loncar, "Deterministic design of wavelength scale, ultra-high Q photonic crystal nanobeam cavities," *Opt. Express*, vol. 19, no. 19, pp. 18529–18542, Sep. 2011.
[31] Q. Quan, P. B. Deotare, and M. Loncar, "Photonic crystal nanobeam cavity strongly coupled to the feeding waveguide," *Appl. Phys. Lett.*, vol. 96, no. 20, May 2010, Art. no. 203102.
[32] D. Yang, C. Wang, and Y. Ji, "Silicon on-chip one-dimensional photonic crystal nanobeam bandgap filter integrated with nanobeam cavity for accurate refractive index sensing," *IEEE Photon. J.*, vol. 8, no. 2, Apr. 2016, Art. no. 4500608.
[33] Q. Huang, K. Jie, Q. Liu, Y. Huang, Y. Wang, and J. Xia, "Ultra-compact, broadband tunable optical bandstop filters based on a multimode one-dimensional photonic crystal waveguide," *Opt. Express*, vol. 24, no. 18, pp. 20542–20553, Sep. 2016.
[34] F. Xia, M. Rooks, L. Sekaric, and Y. Vlasov, "Ultra-compact high order ring resonator filters using submicron silicon photonic wires for on-chip optical interconnects," *Opt. Express*, vol. 15, no. 19, pp. 11934–11941, 2007.
[35] W. Bogaerts, S. K. Selvaraja, P. Dumon, J. Brouckaert, K. De Vos, D. Van Thourhout, and R. Baets, "Silicon-on-insulator spectral filters fabricated with CMOS technology," *IEEE J. Sel. Topics Quantum Electron.*, vol. 16, no. 1, pp. 33–44, 2010.
[36] X. Wang, W. Shi, H. Yun, S. Grist, N. A. F. Jaeger, and L. Chrostowski, "Narrow-band waveguide Bragg gratings on SOI wafers with CMOS-compatible fabrication process," *Opt. Express*, vol. 20, no. 14, pp. 15547–15558, Jul. 2012.
[37] D. Yang, H. Tian, and Y. Ji, "Photonic crystal nanoslotted parallel quadrabeam integrated cavity for refractive index sensing with high figure of merit," *Photon. Nanostruct.-Fundam. Appl.*, vol. 15, pp. 124–129, Jun. 2015.
[38] J. Jágerská, H. Zhang, Z. Diao, N. L. Thomas, and R. Houdré, "Refractive index sensing with an air-slot photonic crystal nanocavity," *Opt. Lett.*, vol. 35, no. 15, pp. 2523–2525, Aug. 2010.
[39] F. Liang, N. Clarke, P. Patel, M. Loncar, and Q. Quan, "Scalable photonic crystal chips for high sensitivity protein detection," *Opt. Express*, vol. 21, no. 26, pp. 32306–32312, Dec. 2013.

ZHONGYUAN FU received the bachelor's degree in communication engineering from the Beijing University of Posts and Telecommunications (BUPT), Beijing, China, in 2014, where he is currently pursuing the Ph.D. degree with the State Key Laboratory of Information Photonics and Optical Communications. His research interest includes photonic crystals and sensors.

FUJUN SUN received the bachelor's degree in communication engineering from the Chongqing University of Posts and Telecommunications, in 2014. She is currently pursuing the Ph.D. degree with the State Key Laboratory of Information Photonics and Optical Communications, Beijing University of Posts and Telecommunications (BUPT), Beijing, China. Her research interest includes photonic crystals and sensors.

JIAN ZHOU received the bachelor's degree in electronic information science and technology from the Nanjing University of Posts and Telecommunications (NUPT), in 2012. He is currently pursuing the Ph.D. degree with the State Key Laboratory of Information Photonics and Optical Communications, Beijing University of Posts and Telecommunications (BUPT), Beijing, China. His research interest includes photonic crystals and sensors.

HUIPING TIAN received the B.S. and Ph.D. degrees from Shanxi University, Shanxi, China, in 1998 and 2003, respectively. She is currently a Professor with the School of Information and Communication Engineering, Beijing University of Posts and Telecommunications (BUPT), Beijing, China. Her research interests include ultrashort and ultrafast process in the transmission of optics, photonic crystals, and broadband information networking.